REPORT DOCUMENTATION PAGE

READ INSTRUCTIONS BEFORE COMPLETING FORM

1. REPORT NUMBER: NRL Report 7693	2. GOVT ACCESSION NO. / 3. RECIPIENT'S CATALOG NUMBER
4. TITLE *(and Subtitle)*: MARINE FOG OBSERVATIONS IN THE ARCTIC	5. TYPE OF REPORT & PERIOD COVERED: An interim report on a continuing NRL problem.
	6. PERFORMING ORG. REPORT NUMBER
7. AUTHOR(s): S. G. Gathman and R. E. Larson	8. CONTRACT OR GRANT NUMBER(s)
9. PERFORMING ORGANIZATION NAME AND ADDRESS: Naval Research Laboratory, Washington, D.C. 20375	10. PROGRAM ELEMENT, PROJECT, TASK AREA & WORK UNIT NUMBERS: NRL Problem No. A03-14A, WR 033-02-01
11. CONTROLLING OFFICE NAME AND ADDRESS: Department of the Navy, Naval Air Systems Command, Washington, D.C. 20361	12. REPORT DATE: April 8, 1974
	13. NUMBER OF PAGES: 27
14. MONITORING AGENCY NAME & ADDRESS *(if different from Controlling Office)*	15. SECURITY CLASS. *(of this report)*: Unclassified
	15a. DECLASSIFICATION/DOWNGRADING SCHEDULE

16. DISTRIBUTION STATEMENT *(of this Report)*

Approved for public release; distribution unlimited.

17. DISTRIBUTION STATEMENT *(of the abstract entered in Block 20, if different from Report)*

18. SUPPLEMENTARY NOTES

19. KEY WORDS *(Continue on reverse side if necessary and identify by block number)*

Fog droplet measurements
Radon
Lyman-alpha
Marine fog
Arctic fog studies
Psychrometry
Potential gradient

20. ABSTRACT *(Continue on reverse side if necessary and identify by block number)*

Shipboard measurements of meteorology, droplet physics, radiochemistry, and atmospheric electricity are described for three marine fog events which occurred in the Greenland Sea during August and September 1972. These measurements include air temperature, sky and sea surface temperatures, humidity, windspeed, atmospheric potential gradient, atmospheric radon concentrations, droplet concentrations, and droplet size spectrums. A variable-path-length Lyman-alpha absorption humidiometer is described which is used for fine structure analysis of water vapor in fogs.

— continues

20.
Abstracted continued —

In all three events persistent fogs were observed to exist in a subsaturated atmosphere with a relative humidity of less than 95% during sizeable portions of the events. Analysis of the possible instrument errors are presented, but these do not negate the findings in the report.

The hypothesis that these observations were the result of the long measurement times required for psychrometry in a structural fog (which consists of alternate pockets of dry and saturated air) was rejected when the Lyman-alpha humidiometer failed to register any large variation in water vapor density. It is also shown that these fog observations cannot be explained as the result of the growth of salt nuclei to equilibrium sizes in the subsaturated marine atmosphere. The current values of droplet evaporation rates do not allow for the possibility of the droplets being formed at higher altitudes under supersaturated conditions and falling to the observation point. It is concluded that our current knowledge of fog physics is not complete when applied to the marine atmosphere.

CONTENTS

MARINE FOG OBSERVATIONS IN THE ARCTIC

INTRODUCTION

In the general field of fog research, marine fog is one important area in which physical documentation is sparse. There exist numerous descriptions of radiation fogs and coastal advection fogs together with models which attempt to describe the formation, behavior, and dissipation of these kinds of fogs. However, because of the difficulties and expense of operations at sea, fog researchers have concentrated on the characteristics of fogs as they appear over or near land. Limited available data suggest that there are important differences between these fogs and those which form over the open ocean. It is therefore important to know some of the characteristics of marine fogs in which ships and aircraft must operate.

As fogs are studied in detail it is becoming obvious that there are important differences both in the way individual fog events are generated and in their microphysical makeup. These differences can affect the modification of fogs in relation to particular modification techniques. An exploratory investigation intended to provide guidelines for planning future observations of marine fogs was made on the USNS *Mizar*. The cruise yielded data which raise questions about some aspects of our present understanding of arctic marine fogs.

EXPERIMENT

In the summer of 1972 the USNS *Mizar*, while on arctic operations primarily oriented toward experiments other than fog, served as a floating platform on which some fog studies were carried out. A meteorological and microphysical data watch was maintained from August 19, 1972 to September 12, 1972. During this period various parts of the Norwegian Sea and the Greenland Sea were traversed as shown in Fig. 1. The dates indicated along the track mark the positions occupied by the vessel at time t = 0001 GMT. The dates of September 4 through September 8 are unique in that during this period the ship was inside the arctic ice floe. The large sea surface temperature gradients encountered in this region are responsible for the high probability of arctic advection fogs.

Three documented fog events are presented here. They are representatively labeled "A" for the event which occurred over open water on August 31, 1972, "B" for the event which occurred in the ice pack on September 4 and 5, 1972, and "C" for the fog event occurring on September 10 and 11, 1972 just east of the ice pack.

Throughout the voyage standard meteorological data were obtained. When a fog was observed, additional instrumentation was used, as manpower permitted, to study the changes in the droplet size spectra with fog age.

Manuscript submitted November 6, 1973.

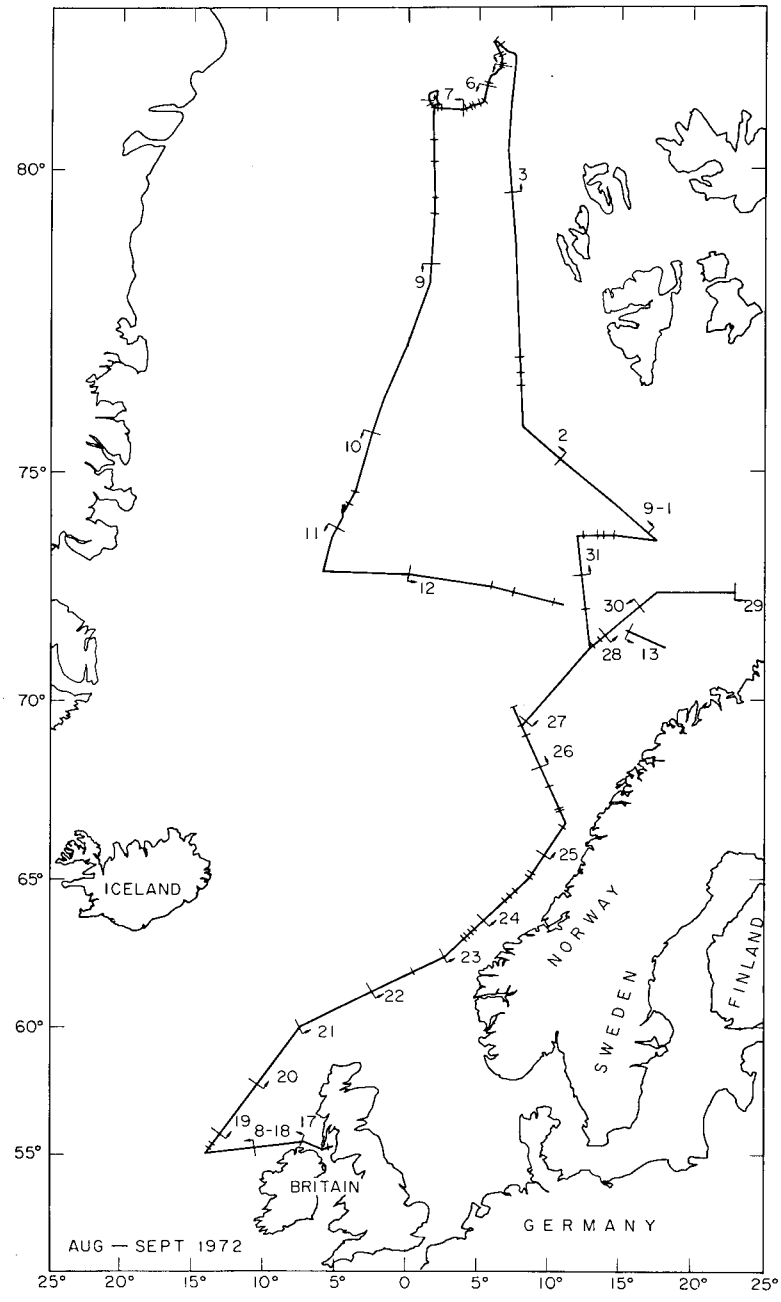

Fig. 1 — Course traversed by USNS *Mizar* for fog studies, August 19 to September 12, 1972

Operations on a ship have certain inherent problems (such as salt, spray, high humidity, and severe motion) associated with the deployment and maintenance of accurate instrumentation. Continuous accurate atmospheric observations are difficult to maintain for long periods at sea. For this reason the bulk of the instrumentation used on this cruise consisted of portable instruments which were kept in the safety of the ship's laboratory except during the actual observations. Most of the data are based on observations taken on the hour.

INSTRUMENTATION

The meteorological watch obtained hourly recordings of dry- and wet-bulb temperatures from a sling psychrometer, sea surface and sky temperature from a hand-held infrared thermometer, windspeed and direction, cloud cover and sea state, and black-and-white and color photography of the horizon. Additional continuous automatic measurements of windspeed and atmospheric electrical potential gradient were recorded throughout the cruise. Samples of atmospheric radon were obtained at 2- to 4-hr intervals throughout the cruise when conditions permitted.

The routine humidity measurements were made with a standard Weather Bureau type of sling psychrometer containing a matched pair of thermometers. Except during measurement times, the instrument was stored in a watertight container to guard against salt contamination of the wick. In addition, distilled water was used in liberal quantities during the wick-wetting procedure in an attempt to wash out completely any salt which may have been picked up in the previous sampling period. All of the measurements were made at deck level on the windward side of the ship and therefore pressure dependent errors were minimized.

Radiational errors and errors from insufficient ventilation, if they exist, can be expected to raise the wet-bulb temperature and hence cause the relative humidity reading to be too high. Under the existing conditions radiation could not be expected to cause the measure of relative humidity to be too low. Heat conduction from the apparatus to the wet bulb can also cause errors with the psychrometer. The net effect for any heat conduction error is to increase the observed relative humidity. During fog the possibility of fog droplets being deposited on the dry bulb exists. Here again the net effect on the observation of relative humidity is to increase the apparent value to readings above the true value. During periods of severe pitching and rolling, the observer attempted to stay clear of the spray. The temperatures were read to the nearest 0.2°F.

The routine dry- and wet-bulb humidity measurements, being important to our understanding of fogs, were supplemented and checked by two other types of humidity instruments. During a nonfoggy period at the ice edge, dewpoints computed from the hourly dry- and wet-bulb temperatures were compared to those indicated by the Cambridge Systems Marine dewpoint hygrometer mounted beyond the bow upwind of the ship. Air temperatures were within 0.2°C of each other but the hygrometer registered an average dewpoint that was 0.4°C lower than that computed from the sling psychrometer measurements. This was as expected since we had already considered that the errors inherent in the psychrometric humidity determinations are all in the direction of registering more relative humidity than is actually present.

A third humidity measurement based upon the optical absorption of Lyman-alpha radiation was incorporated into the experiment. The Lyman-alpha instrument, described in Appendix A, is capable of a very fast response to fluctuations in water vapor density even during fog conditions. The actual calibration of this device at sea was obtained by finding the linear regression relationship between the output signal of the absorption device to the vapor density calculated by the dry- and wet-bulb sling psychrometer over the entire period when both sets of data were simultaneously available. For a sample size of 36 data pairs, a correlation coefficient of 0.83 was obtained. With this calibration the absorption instrument was used to probe the small-scale behavior of the water vapor density during a fog. With the recorder used on the ship, events with a time scale on the order of 2 s could be resolved. It should be noted that this is entirely the response time of the recorder. The response of the Lyman-alpha device itself is about 1 ms and on the order of 0.01 s when including changing the sample.

FOG DROPLET MEASUREMENTS

In addition to the hourly meteorological observation, fog droplet samples were obtained by means of a hand-held impactor similar to that described by Mazé et al. [1] and used by Ruhnke [2]. This instrument incorporates a spring-loaded piston which takes in 25.8 cc of calm air in 0.01 s through a rectangular slit nozzle and impacts droplets on a glass slide coated with newly deposited magnesium oxide. Ranze and Wong [3] have determined the efficiency of impaction for various size aerosols for the geometry of a finite rectangular jet impinging on a flat plate. Figure 2 is a plot of the efficiency of impaction with respect to aerosol size for the physical dimensions and velocities present in the particular impactor used for this investigation. It appears from this plot that all particles with diameter greater than 2.0 μm are impacted on the slides. Accurate detection and sizing of these very small droplets present a more difficult problem. Through a series of experiments it was determined that the droplet deposition density was not uniform throughout the slide. The actual contours of the droplet deposition density function could be fairly well represented by a series of ellipses all sharing the same foci, with the line passing through these foci being parallel to the slit.

In order to make sure that all sizes of impacted droplets were equally accounted for, a series of consecutive photomicrographs of the slide was taken, forming a strip of surface area perpendicular to the length axis of the rectangular jet and running from one edge of the slide to the other. This strip was taken approximately midway between the ends of the jet to minimize edge effects. Each photomicrograph had a magnification of 110× and represented a 483- × 654-μm surface. The droplets on this strip represent those found in a constant fraction of the total sampled air. The entire strip contained about 20 individual photomicrographs, each of which was manually scanned to obtain the droplet size distribution.

The accuracy of the size measurements made with an impactor depends on the calibration of the collection surface. May [4] obtained a calibration for magnesium oxide based on the ratio between the diameter of the observed impaction circles on the slide and absolute diameters of the droplets themselves. May's calibration was for droplets greater than or equal to 9.9 μm in diameter. He states that below this size, the magnesium oxide method is of little value for measurement purposes because of grain size of the MgO surface; although for high velocities, sizes of less than 5 μm are observed.

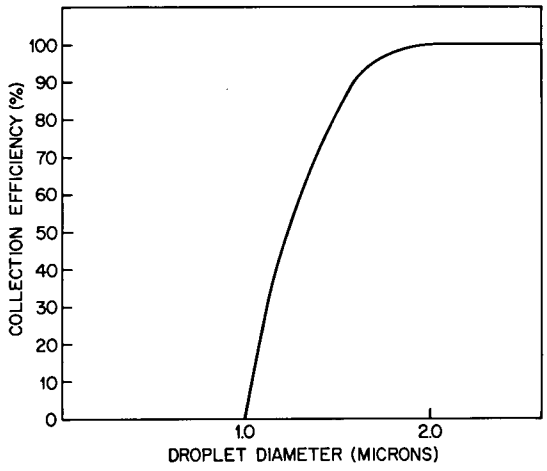

Fig. 2 — Plot of the collection efficiency of the impactor used for fog droplet sampling

During the sampling process, the impactor used in this fog study had an air velocity at the jet of 74 m/s. This velocity is apparently high enough to cause large quantities of small droplets to leave their impressions on the freshly prepared magnesium oxide slide used in this experiment. These impressions were viewed using oblique lighting where light-dark patterns of the droplet crater are easily identifiable. Consequently, a linear extrapolation of May's calibration curve was used to obtain droplet sizes below 10 μm from the images formed in the magnesium oxide surface.

In order to check the validity of this extrapolation, a comparison was made between the impactor and an axially scattering cloud-droplet-size spectrometer designed by R. Knollenberg and manufactured by Particle Measuring Systems, calibrated with glass spheres of known size. The source of the water fog for this comparison was an ultrasonic transducer aerosol generator. The impactor slide was processed in the same way as the slides used in the shipboard experiment with image size intervals of 9 μm. The counts from the more detailed spectrum of the axially scattering system were divided to compare with the same intervals as obtained from the impactor. For this comparison, the range used for the axially scattering instrument was from 3 to 31 μm. The results of the comparison are shown in Fig. 3. The corrected size distribution data obtained with the impactor were used to calculate both the liquid water content of the fog and the visibility, using the following formulas.

$$\text{l.w.c. } (\text{mg/m}^3) = \frac{1.33\,\pi \sum_{n=1}^{\infty} r_n^3\, f_n\, \rho}{\text{Sampled Volume } (\text{m}^3)}$$

$$\text{visibility (m)} = \frac{7.8 \text{ Sampled Volume } (\text{m}^3)}{4\,\pi \sum_{n=1}^{\infty} r_n^2\, f_n}$$

where

ρ is density of water in mg/m^3

r_n is the midsize of the nth size interval expressed in meters

f_n is the number of droplets in the nth size interval

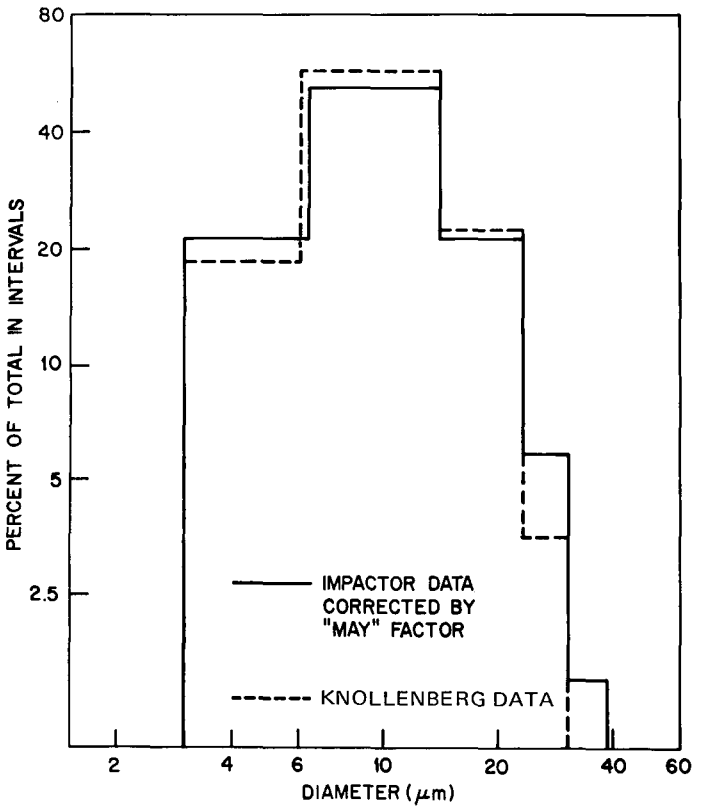

Fig. 3 — Comparison between droplet size spectra obtained with the impactor and the spectra measured with Knollenberg's axially scattering aerosol spectrometer

ATMOSPHERIC RADON

Atmospheric radon (^{222}Rn) was measured throughout the voyage when conditions were suitable as indicated by the unnumbered crosshatches in Fig. 1. Radon has been frequently used as an air mass tracer; for example, Reiter [5] characterized air masses arriving in central Europe by radon content and Rama [6] used radon concentration as an indicator of a continental contribution to monsoon air masses.

Radon is of particular interest in marine fog experiments as a tracer of continental air masses arriving at the ship, since the radon contribution from the sea is very small. Its relatively short half-life (3.82 days) insures us that a high measured peak in radon concentration can result only if this air mass had recently been over land. It was shown by Larson et al. [7] that continental dust is associated with unusually high radon concentrations and that calculated air mass trajectories are consistent with the radon and dust having been transported by air masses that moved recently from continental areas. An important distinction to bear in mind is that dust can be removed by precipitation and settling; thus it is possible (and it has been observed) to have radon but no dust, yet the converse has not been observed. Dalu and Dalu [8] have shown that the only process that eliminates radon from the atmosphere is radioactive decay.

The radon measurement consisted of collecting radon daughter products on filter paper and indirectly determining the radon concentration from the beta radioactivity of the daughter products, using a technique described in detail by Larson [9]. This method offers simplicity and sensitivity but requires relatively good weather conditions because equilibrium between radon and its daughter products is assumed. Thus there is the possibility that rain and/or fog may remove daughter products from the atmosphere, and thus result temporarily in erroneously low indicated values for radon concentration. The radon concentrations over the oceans (and hence counting rates) are too low to enable an estimate of disequilibrium from the shape of the decay curve of the daughter products. Equilibrium is restored in about 2 hr after the end of the removal of the daughter products. In rough seas it was impossible to set up the sample collector at the bow of the ship.

Constant-pressure hemispherical charts are usually used for estimating the trajectories of air masses. Surface, 700-mb, and 500-mb charts generally give very similar trajectories, with motion often being the greatest at 500 mb. It is assumed that each 12-hr constant-pressure chart represents a pressure wind system of 12 hr, and that the 12-hr displacement was computed upstream using the geostrophic wind equations for constant-pressure charts. This calculation of air mass trajectories is complicated because of the many successive extrapolations. Occasionally, the calculated trajectories are different for each level. If the systems are not well defined, it is possible to start at two points very close together and end with substantially different origins for the air mass. It is at this point that radon measurements are of importance in ascertaining the correct trajectory.

Radon measurements are shown in Fig. 4 and the concentrations measured during fog events A, B, and C are presented in Table 1. Several peaks (August 24, 25, 31 and September 5, 6, 8) were recorded and are similar to the "radonic storms" observed by Lambert et al. [10] in Antarctic areas. After the sharp pulse of August 31, data were recorded more frequently when conditions permitted. A similar cruise in 1971 had shown little evidence of large-value, short-term fluctuations.

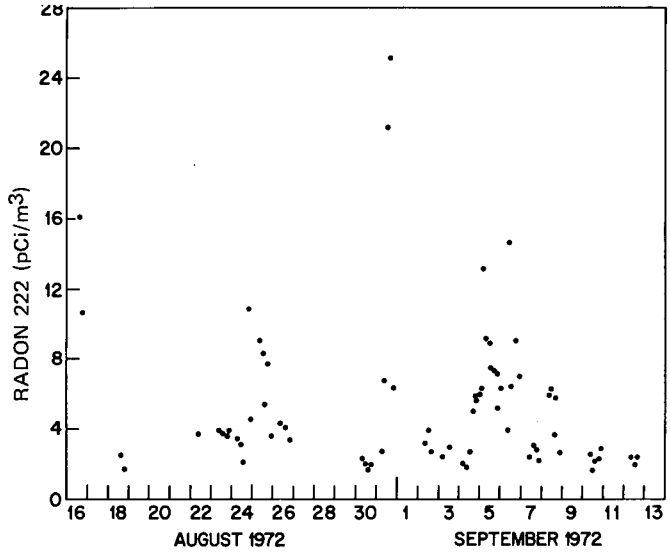

Fig. 4 — Radon measurements made during the cruise

Table 1
Radon Concentrations

Date	Time	Activity (pCi/m^3)	Fog Event
Aug. 31, 1972	845	2.75	A
	1000	6.80	A
	1200	21.30	A
	1300	25.20	A
	1730	6.32	A
Sept. 4, 1972	845	2.06	B
	1045	1.91	B
	1300	2.75	B
	1800	5.07	B
	1840	5.94	B
	2200	5.75	B
	2330	5.93	B
Sept. 5, 1972	0200	6.34	B
	0400	13.20	B
	0600	9.15	B
	0845	9.06	B
	1200	7.49	B
	1515	7.35	B
	1800	7.33	B
	2200	5.19	B
Sept. 10, 1972	1030	2.73	C
	1340	1.68	C
	1600	2.28	C
	1800	2.35	C
	2210	3.02	C

Comparison of radon dust and air mass from this cruise [11] and some Antarctic data [12] reinforce the conclusion by Larson et al. [7] that unusually high dust and radon concentrations observed over the ocean result from air masses that were recently over continental areas. Further, there are indications that the peaks in radon are associated with frontal systems. Unfortunately the large volume of air necessary for dust measurements requires many hours of sampling time and the time-vs-concentration relationship has not been established for dust. Dust samples can be taken only when there is no fog or precipitation; thus there can be no concurrent dust-vs-fog relationships although some inclusive attempts have been made to analyze fog water for the characteristic components of continental dust. From this and previous data [7], it appears that the "normal radon background" in the Norwegian and Greenland seas is about 3 pCi/m^3. This background is probably due to the nearness of large continental areas because the radon concentration over the ocean in the southern hemisphere can be as low as 1/2 pCi/m^3 or less [6,13].

Although radon is a radioactive element that produces atmospheric ions on disintegration, its effect on atmospheric electrical conductivity (assuming the peaks in concentrations of less than 30 pCi/m^3) can be more than compensated for by the addition of continental dust pollutants which attach to the mobile small ions and hence can reduce the atmospheric conductivity.

INTERPRETATION OF ATMOSPHERIC ELECTRICITY DATA IN FOGS

The potential gradient is a parameter which responds to many influences remote from the sensor, but is chiefly generated as a result of worldwide thunderstorm activity. The atmospheric potential gradient at the ocean surface has a nominal value of 100 V/m. Global phenomena are known to cause variations of no more than 50%. Local and mesoscale phenomena on the other hand can superimpose a much greater range of values of potential gradient. In an attempt at filtering out the global scale phenomena, we will consider only values of 200 V/m or greater as significantly different from normal to insure that we are indeed observing the potential gradient superimposed by local or mesoscale atmospheric phenomena in the immediate vicinity of the ship.

Although the interpretation of electrical parameters by themselves contains ambiguities as to the exact cause of anomalous electrical effects, a suitable complement of other measurements made simultaneously with the electrical measurements can provide information which can be otherwise very difficult to obtain. Gathman and Trent [14] describe the problem of anomalously high potential gradient measurements on board a ship resulting from the charged stack gas plume. If, however, the ship speed, relative wind direction, and windspeed are known, then the effect of the stack gas plume can be accounted for. By being mindful of this problem, the experimenter knows when the potential gradient is dominated by the component of electric field due to the stack gas and can either omit these data or change the course or speed of the ship. Fortunately, during all three fog events reported here, the ship speed and relative wind direction were such that the problem of the stack gas charge was minimized. We feel that at least the gross electrical effects noted are the result of local natural atmospheric electric phenomena and not that of the ship.

In a homogeneous air mass an electrical current is flowing continuously to ground. This current originates from the combined action of worldwide thunderstorm activities and is distributed throughout the world by the high-altitude conducting layers. The net current flow in any one area depends on the columnar resistance of the entire atmospheric column from the earth's surface to the ionosphere. If a small layer within this column has an increase in resistance (a decrease in conductivity), then the net current decreases only slightly but the potential gradient throughout the high resistance layer increases according to Ohm's law, and there is a continuity of current flow. Therefore, if atmospheric conductivity is low in the layer next to the earth's surface for some reason, there is a relatively high electric potential gradient present. In the arctic marine atmosphere, the electrical conductivity is chiefly the result of small ions being produced by cosmic radiation. Normally this air, being very pure, has an Aitken nucleus count of at most a few hundred particles per cc, and the reduction of conductivity resulting from ion-aerosol attachment is small. The addition into the atmosphere of fog droplets provides a larger specific surface area for the diffusional loss of ions and effectively reduces the conductivity of the air. Accordingly, the formation of fog droplets over the level sea causes increases in ambient electric field by a factor of perhaps 2 or 3. This phenomenon is well known, and a number of investigations have reported it [15].

FOG EVENT A

Figure 5 displays a plot of the measured parameters just preceding the fog event of August 31, 1972 and during the initial phases of the event. At this time the ship was near 74°N, 13°E. The position and warm sea surface indicate that the ship was in the Norwegian current. Earlier in the day, the surface wind was out of the south moving at a speed of 13 knots. About 6 hr before the visible onset of the fog, the wind direction veered to the southeast for a period of 3 hr or so, then changed to the southwest, whereupon the surface windspeed increased to 17 knots. Coincident with the change in the wind vector, the initially clear sky became completely overcast. This was also observed within the sky temperature data, which during clear conditions indicated temperatures less than −20°C. But several hours before the fog, the sky temperature increased rapidly to coincide exactly with the sea surface temperature at the time of the initial occurrence of visible fog. This same phenomenon for coastal advection fogs was noted by Mack et al. [16] at Vandenberg AFB in California. The radiational cooling was obviously nonexistent or small at the time of fog formation as is indicated in Fig. 5 by the sea and sky temperatures being identical. The atmospheric electric precursor effect [17] was present during this event as indicated by the large potential gradients measured before the onset of fog between 1430 GMT and 1600 GMT on August 31, 1972. At 0900 GMT the ship encountered an anomalous tongue of air which was identifiable by an order of magnitude increase in radon gas concentration along with a wind change toward southeast. Radon, atmospheric dust, and air mass trajectories [11] are consistent with this air having passed over northwest Scandinavia within 2 days. Dust collection was discontinued at the onset of fog.

At 1600 GMT visible fog was encountered at the same time the relative humidity reached 100%. As time progressed, the subjectively observed fog gradually lessened in density until about midnight when only a mist was observed. Throughout the duration of the fog, the windspeed was relatively high and the air temperature less than the water

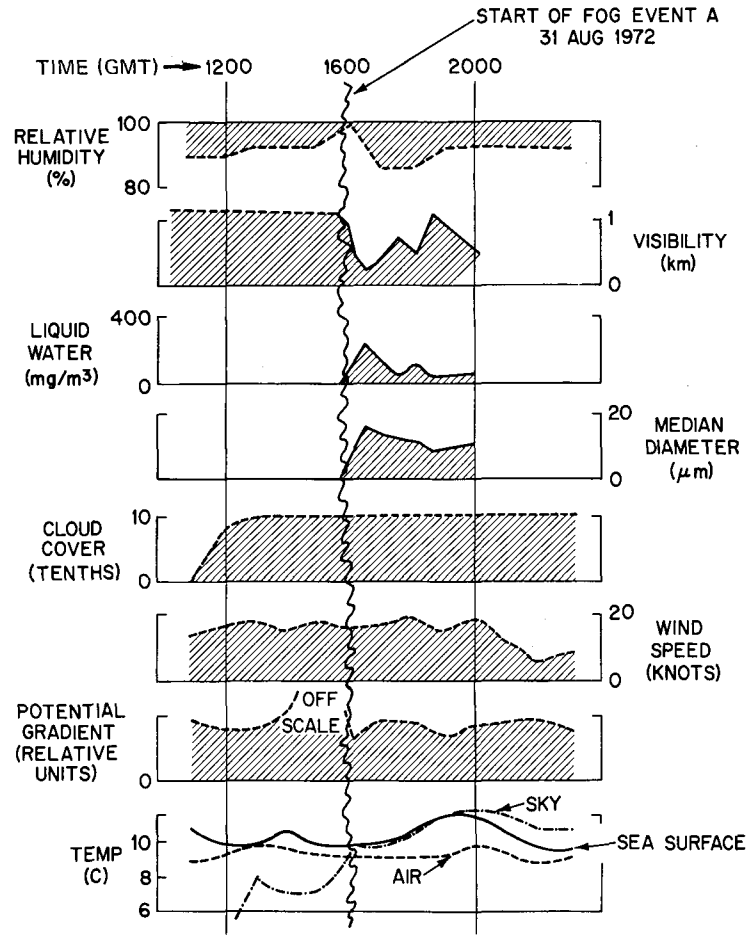

Fig. 5 — Measured parameters preceding and during fog event A

surface temperature, indicating a well-mixed atmosphere. One and one-half hours after the initial appearance of the fog, the radon concentration had dropped a factor of four, but was still about twice "normal," suggesting that the ship was moving out of the tongue of air or frontal system or that the stability of the atmosphere was reduced. The actual radon concentration at this time could have been higher since the fog could have removed many of the radon daughter products as suggested earlier.

FOG EVENT B

Figure 6 shows the course of the variables throughout fog event B occurring on September 4 and 5, 1972. At this time the ship was in the ice floe, and the water temperature was -1°C, with floating ice chunks occupying about 50% of the sea surface. These ice chunks were wet, and the infrared thermometer indicated their surface temperatures to be within 0.5°C of the surrounding water. There is little or no wave motion in the ice floes since swells originating elsewhere are effectively damped by the ice. The question arises as to whether this fog is a warm or a supercooled or partially frozen (ice)

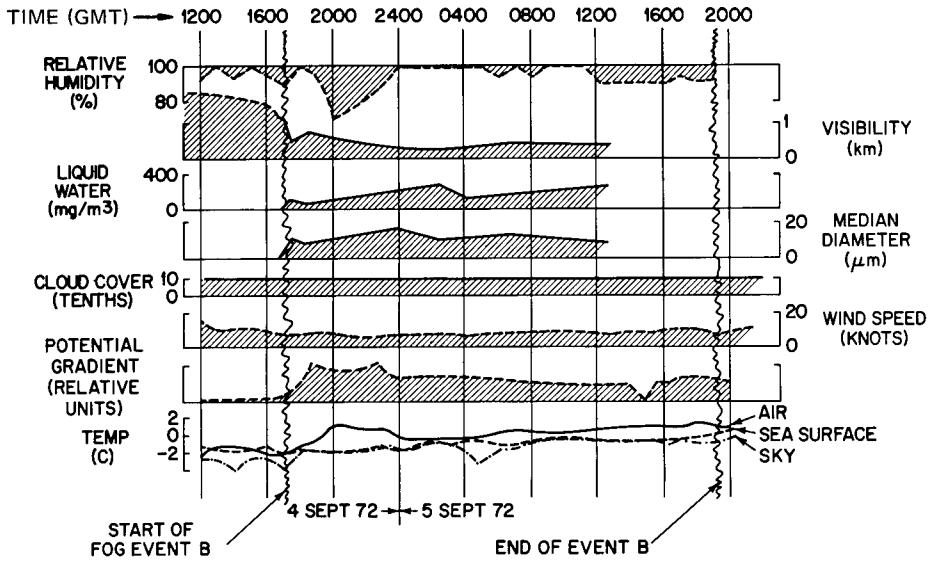

Fig. 6 — Measured parameters for fog event B

fog. Initially, at the first visual observation of the fog, the air temperature was slightly below freezing. However, more than half of the time throughout the duration of this fog, the air temperature was 0°C or above.

Prior to the fog, air temperature and the water surface temperature were approximately equal, indicating a neutral lapse rate. During the fog however, the air temperature was significantly greater than the sea temperature, indicating stable atmospheric boundary conditions. Prior to and during the event, the sky was overcast and the sky and sea surface temperatures were similar, precluding any radiation effects. The potential gradient increased abruptly just before the visual observation of fog, and remained relatively high throughout the duration of the event, with the exception of a sharp local minimum at 1400 GMT on September 5, 1972. On several occasions during these fog events, it was noted that short periods of rain produced recordings of negative potential gradient. When the rain stopped, these immediately returned to the high positive values usually observed in the fog. It should be noted here that the potential gradients presented in Figs. 5, 6, and 7 are averaged over 1 hr; therefore these brief sign reversals appear only as lower positive values. Between 1930 GMT and 2300 GMT on September 4, 1972, a relative humidity of 75% was observed. During this interval actual impactor samples were not taken, but the observer reported medium to heavy fog. The potential gradient measurement exhibited a local minimum while the air temperature measurement showed a local maximum during this same period of time.

The normal radon background activity for the Arctic region is about 2.5 pCi/m^3. Simultaneously with the appearance of the fog (1730 GMT) on September 4, the radon activity doubled and remained two to five times normal throughout the fog event. Surface, 700-mb, and 500-mb air mass trajectories were self-consistent each day. At 1200 GMT on September 4, the air had spent at least 7 days over ice-covered or ocean areas. By 1200 GMT on September 5, the new air parcel had passed over Scandinavia only 2 or 3 days before. No dust data were taken.

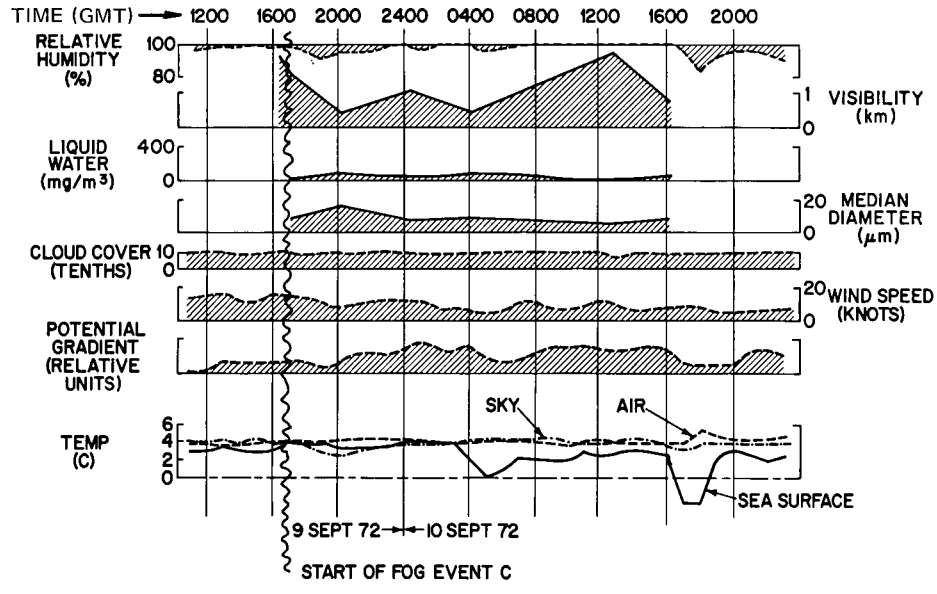

Fig. 7 — Measured parameters for fog event C

FOG EVENT C

Figure 7 shows event C, which was observed while steaming south in open water along the east coast of Greenland. On September 10 and 11, two tongues of cold surface water were encountered as is seen by minima in the sea surface temperature at 0330 GMT and at 1730 GMT on September 10. The wind averaged about 10 knots during this fog event. The relative humidity and the potential gradient also indicated local minima which corresponded to these tongues of cold water. Unfortunately the droplet size spectra are not closely enough spaced to determine the effect of these cold water tongues on the microphysics of the fog.

In general, it appears that from 0400 to 2400 GMT on September 10, the air temperature was significantly higher than the sea surface temperature, indicating a stable atmosphere. Five radon samples were taken between 1100 and 2400 GMT on September 10 and all of these indicate normal arctic values of about 2.5 pCi/m^3 with no indication of continental air mass. The atmospheric electric precursor effect was not observed at all during this fog although after four or five hours of fog age, the potential gradient did reach the characteristic "high" values usually observed in fogs.

Table 2 lists some of the characteristics of the droplet size distributions obtained during events A, B, and C. These distributions are not unlike the coastal advection fogs reported by Mack et al. [16]. The average droplet diameter of the three arctic marine fogs was 13.6 μm while the average droplet concentration was 20.7 droplets per cubic centimeter. Actual droplet size distributions are presented in Figs. 8, 9, and 10.

Table 2
Fog Droplet Size Distributions

Event	Date	Time	Droplet Density (drops/cc)	Spectrum Median Diameter (μm)	Calculated Visibility (m)	Calculated Liquid Water Concentration (mg/m^3)
A	Aug. 31	1630	18.4	16.8	224	224
A	Aug. 31	1730	13.3	12.8	740	43
A	Aug. 31	1810	15.5	11.8	457	95
A	Aug. 31	1835	11.9	9.1	1112	29
A	Aug. 31	2000	25.6	12.3	447	65
B	Sept. 4	1730	15.5	10.9	420	100
B	Sept. 4	1830	26.3	7.6	674	41
B	Sept. 5	0001	29.8	17.9	208	184
B	Sept. 5	0230	47.3	10.2	179	251
B	Sept. 5	0400	46.9	10.3	267	111
B	Sept. 5	0630	25.2	13.0	344	144
B	Sept. 5	1235	39.5	8.6	219	214
C	Sept. 9	1700	11.4	8.2	1480	20
C	Sept. 9	2000	15.9	14.4	430	93
C	Sept. 10	0015	10.1	6.3	1000	42
C	Sept. 10	0400	26.7	8.4	460	85
C	Sept. 10	1230	5.8	5.4	2070	19
C	Sept. 10	1600	15.1	8.6	726	51

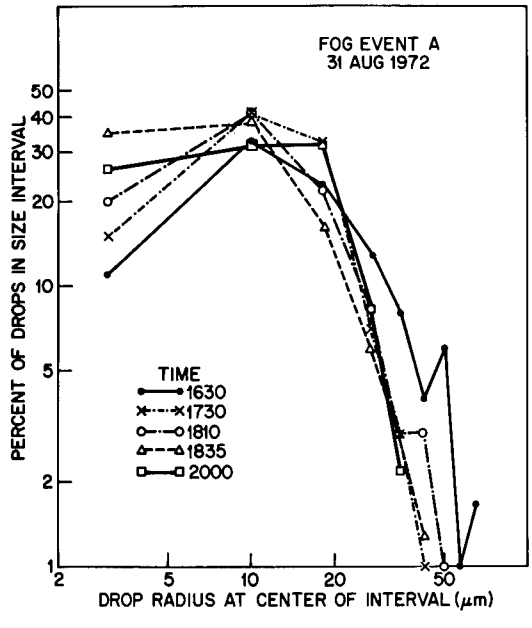

Fig. 8 — Fog droplet size distributions, fog event A

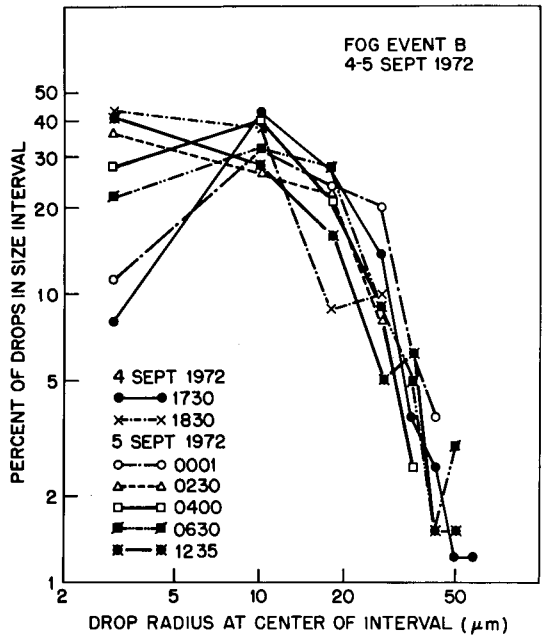

Fig. 9 — Fog droplet size distributions, fog event B

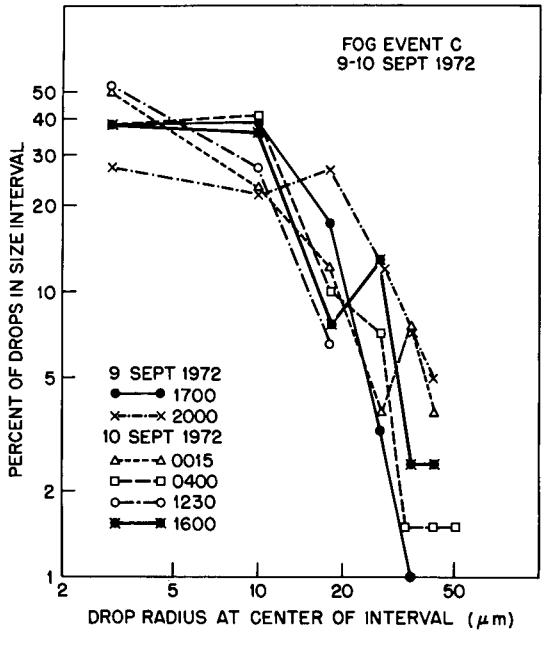

Fig. 10 — Fog droplet size distributions, fog event C

DISCUSSION OF EXPERIMENTAL DATA

We have discussed the meteorological data obtained during fog events "A," "B," and "C." The data indicate that these fogs differ from each other in aspects as to their microphysics, the meteorological conditions during and just preceding their formation, and the possible influences related to the presence of a continental air mass. These areas of study alone highlight the many differences in natural fogs which occur even in such a homogeneous region as the Norwegian and Greenland seas.

One common feature of these data, however, is that at the time of the initial shipboard observation of the fogs, the observed relative humidity was 100%. Yet, in all three cases observations of the relative humidity taken from the sling psychrometer indicated that during considerable portions of the fogs relative humidities of less than 100% were measured. These peculiar dry readings occur even during periods when heavy persistent fog was captured with the impactor. This implies that indeed many fog droplets were existing in the atmosphere simultaneously with less than saturated conditions. Similar results were obtained by Mack et al. [16] in their observations of advection fogs on the California coast. They attributed the observed differences between the dewpoint and temperature in the fog to be the result of the drift in the calibration of the dewpoint measuring system.

In the case of experimentation covered in this report it is difficult to attribute the observed phenomenon to errors in the operation of the sling psychrometer because, as discussed earlier, the errors in this simple instrument tend to cause readings of relative humidity values that are too high rather than too low. It is also significant that results were obtained independently of the operator, i.e., low humidities were obtained by all four scientists who stood watch on the *Mizar* cruise. Such measurements might be explained if the fog were structured and consisted not only of pockets of supersaturated air in which fog existed, but also drier eddies in which fog droplets did not exist. Such a structure was not noticed by the observers. The nature of the sling psychrometer requires slinging the device for a period of several minutes; therefore, an average relative humidity would be observed which was averaged over both dry and wet pockets. On the other hand, between two and five individual samplings taken quickly in consecutive order were deposited on an individual slide with the impactor in order to obtain a sufficiently high droplet density to analyze. Thus, these slides would probably not reveal any subsaturated pockets but record only the droplets in the supersaturated pockets.

To investigate the plausibility of this explanation, the fast response record of the Lyman-alpha absorption humidiometer was studied during one of the periods when fog existed concurrently with the low humidity measured by the sling psychrometer. During the period of 0530 to 0630 GMT on September 5, fluctuations in water vapor density measured with the Lyman-alpha device had a standard deviation about the mean of only 0.5%. If we assume that dry-air temperature remained constant over the period, this is equivalent to a 1% variation in relative humidity and much less than needed to account for the structure fog model proposed above.

Humphreys [18] offers an explanation for this phenomenon by his statement "Fogs at sea, of various density, must often occur while the humidity still is distinctly below that of saturation, owing to the presence of the highly hygroscopic sea-salt dust."

We have attempted to verify this explanation of the observed phenomenon by comparing an estimated sea-salt size distribution for the meteorological conditions encountered during specific fog event A with the measured fog droplet size distribution. The estimation of the sea-salt size distribution is based on Woodcock's measurements [19] of salt nuclei in the marine air taken at an altitude of approximately 700 m and presented as a function of wind force measured at 10 m above the sea surface. We extrapolated these values to the sea surface by following the method used by Toba [20]. The final step was to convert the salt nucleus weights at the surface to the equilibrium sizes that NaCl particles would obtain at the measured relative humidity [21]. The resulting sea surface distribution of salt nuclei at 95% relative humidity and a wind force of 5 is given in Fig. 11 where it is compared with the measured fog droplet size distribution at 1630 GMT on August 31, 1972. The order of magnitude difference between these two distributions makes it difficult to accept the hypothesis that we were only observing sea salt haze at these times.

It is equally hard to imagine that what was observed were the remains of droplets formed overhead in a supersaturated region which had fallen to the subsaturation region near the sea surface, as the evaporation times for the observed droplet sizes are too short.

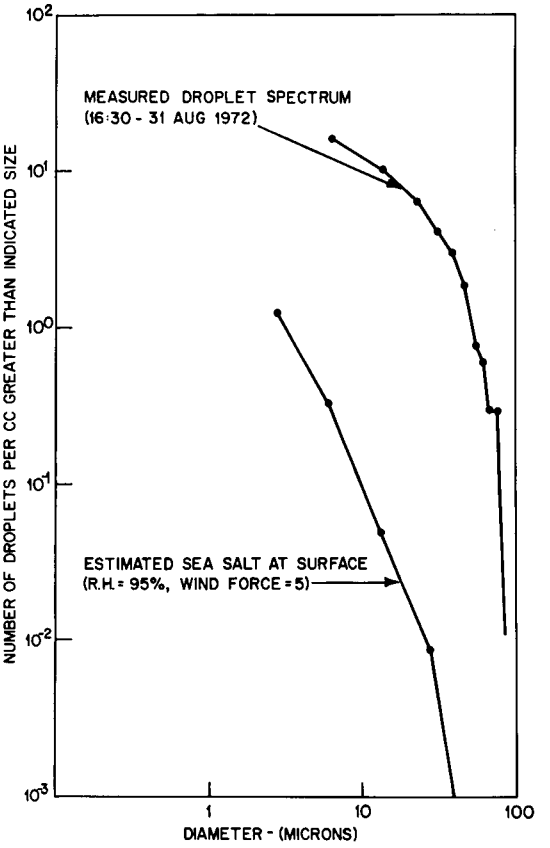

Fig. 11 — Comparison of calculated distribution of sea-salt nuclei with measured fog droplet size distribution

For instance, the 20-μm-diameter droplet has an evaporation time of about 10 s at a relative humidity of 95% (Jiusto [22]) during which time it can fall no more than 11 cm.

In conclusion it can be said that we can not explain these marine fog observations in a consistent way on the basis of current knowledge of fog physics. It is obvious that more fog measurements at sea are essential if we are to unscramble these seemingly contradictory observations and to proceed in an orderly fashion to understand the formation and dissipation of marine fogs.

ACKNOWLEDGMENTS

We wish to thank Messrs. R. A. Carr and D. J. Bressan who in addition to their other duties shared in the maintenance of the meteorological data watch throughout the cruise. We wish to thank Dr. S. H. Brown of the Arctic Submarine Laboratory, particularly for the use of his dewpoint data presented in this report.

We are especially indebted to Mr. Robert Ruskin and Dr. James Fitzgerald for previewing the manuscript and helpful discussions.

We also wish to thank Mr. Charles Votaw (Senior Scientist on Board) and the officers and crew of the USNS *Mizar* for their cooperation.

REFERENCES

1. R. Maze, J.R. Paugam, and R. Serpolay, *Proceedings of the 7th International Conference on Condensation and Ice Nuclei*, Prague and Vienna, Sept. 18-24, 1969.
2. L.H. Ruhnke, "Fog Droplet Sizes at the Panama Canal," NOAA-TR-ERL 209-APCL 22 (1971).
3. W.E. Ranze and I.B. Wong, Ind. and Eng. Chem. **44**, 1371-1381 (1952).
4. K.R. May, J. Sci. Inst. **27**, 128-130 (1950).
5. R. Reiter, Nukleonik **6**, 313-320 (1964).
6. Rama, J. Geophys. Res. **75**, 2227-2229 (1970).
7. R.E. Larson, R.A. Lamontagne, P.E. Wilkniss, and W.I. Wittman, Nature **240**, 345 (1972).
8. G. Dalu and G.A. Dalu, *Colloquium on the Physics and Chemistry of Aerosols*, Fontenary-Aux Roses, Sept. 24, 25, 1970.
9. R.E. Larson, Nuc. Inst. and Methods **108**, 467 (1973).
10. G. Lambert, G. Polian, and D. Taupin, J. Geophys. Res. **75**, 2341-2345 (1970).
11. D.J. Bressan, R.E. Larson, and P.E. Wilkniss, Nature **245**, 144 (1973).

12. P.E. Wilkniss, R.E. Larson, D.J. Bressan, and J. Steranka, "Atmospheric Radon and Continental Dust near the Antarctic and Their Correlation with Air Mass Trajectories Computed from Nimbus 5 Satellite Photographs," submitted to J. Appl. Meteorol. for publication.

13. P.E. Wilkniss, R.A. Lamontagne, R.E. Larson, J.W. Swinnerton, C.R. Dickson, and T. Thompson, Nature **245**, 142 (1973).

14. S.G. Gathman and E.M. Trent, "Atmospheric Potential-Gradient Measurements at Sea," NRL Report 7030, Feb. 1970.

15. H. Dolezalek, Rev. of Geophys. **1**, 231-282 (1963).

16. E.J. Mack, W.J. Eadie, C.W. Rogers, W.C. Kocmond, and R.J. Pilie, "A Field Investigation and Numerical Simulation of Coastal Fog," NAS 8-27999 (Aug. 18, 1972).

17. G.P. Serbu and E.M. Trent, Trans. Amer. Geophys. Union **39**, 1034-1042 (1958).

18. W.J. Humphreys, *Physics of the Air*, 3rd ed., Dover Publications Inc., New York, 1964, p. 287.

19. A.H. Woodcock, J. Met. **10**, 362-371 (1953).

20. Y. Toba, Tellus XVII, 131-145 (1965).

21. R.D.H. Low, "A Comprehensive Report on Nineteen Condensation Nuclei," Army Electronics Command Report ECOM 5249, Ft. Monmouth, N.J., 1969.

22. J.E. Jiusto, "Nucleation Factors in the Development of Clouds," Ph.D. Dissertation, Penn State University, 1967.

Appendix A

THE LYMAN-ALPHA VARIABLE-PATH-LENGTH HUMIDIOMETER

Figure A1 is a drawing of the essential part of the variable-path-length Lyman-alpha absorption humidiometer. It consists of a detector and a source tube capable of being positioned in either of two positions. The "in" position provides a small spacing between the detector and source tube and in this position the humidiometer is in a calibration mode during which the main absorption is due to coatings on the windows. The air sample is diverted around the source tube. When the movable piston is pulled out of its cylinder as far as the stop will allow, the air sample passes between the source tube and the detector. The absorption is now due to both the window coatings and the water vapor in the air sample. It should be noted that the loss of light because of this change in geometry remains constant for a given source tube and detector pair and is therefore easily corrected.

Several schemes have been used to provide the required positive motion. A system of springs, an eccentric, and a motor were used for the data reported in this report. This proved to be rather cumbersome for operation on the deck of the ship. An improved pneumatic system has now been built which will hopefully overcome the mechanical difficulties experienced during the *Mizar* cruise.

The system used on this cruise utilizes the high absorption coefficient of water vapor in some regions of the vacuum ultraviolet radiation spectrum. The theoretical basis of the operation of these types of instruments is summarized by Tillman [A1], Ruskin [A2] and Randall, et al. [A3]. The instrument used in this experiment incorporates the best of the many technological improvements in Lyman-alpha radiation source tubes, ultraviolet window materials, and Lyman-alpha detectors developed at NRL during the past 15 years. In addition, a reduction in such problems as deterioration by collection of film on windows, changes in the UV radiation spectrum, and detector efficiency was effected by the variable-path-length configuration used.

Calculations have shown that the scattering due to liquid water droplets, even in a dense fog, has little effect on the sensitivity of the vapor absorption in the device because of the short path length used (0.5 cm). Therefore, such a system could be used even in a fog, whereas conventional humidity devices are of questionable accuracy. (The dewpoint instrument cannot distinguish between fog droplets and dew formed on the mirror. Deposited liquid water droplets can completely alter the reliability of other instruments.) One major problem with this Lyman-alpha instrument is that of reduced signal caused by deterioration and/or chemical etching of the ultraviolet transparent windows with time. The absorptive effect of liquid water and/or sea-salt film on the windows themselves is even a greater source of reduced signal for operation of the device in the marine environment. The change in radiation intensity and the detector sensitivity with time are also sources of major concern.

The intensity of radiation received by the detector may be represented by the following integral:

$$I = \int_{\lambda_1}^{\lambda_2} I(\lambda) \exp\left[-\left(\frac{k_1(\lambda)\rho_1}{\rho_{10}} + \frac{k_2(\lambda)\rho_2}{\rho_{20}} + ... + \frac{k_i(\lambda)\rho_i}{\rho_{io}}\right) x\right] d\lambda,$$

where

λ is radiation wavelength

$I(\lambda)$ is the spectrum of incident radiation

k_i values are the absorption coefficients of the major gaseous absorbers in the sample

ρ_i is the density of the ith gas

ρ_{io} is the density of the ith gas at STP (which can be fictitious)

λ_1 and λ_2 are the limits of the pass band of the transmission windows and detector

x is the path length that the radiation must follow through the sample.

If we have a strong Lyman-alpha line of intensity I_L in the hydrogen source tube spectrum at $\lambda = \lambda^1$, we may represent $I(\lambda)$ by the sum of a delta function and a continuous spectrum, as

$$I(\lambda) = I_L\ \delta(\lambda - \lambda^1) + I_c$$

where I_c is the energy in the continuous portion of the spectrum. There is also good justification for considering only the absorption of H_2O vapor and O_2 gas with the subscripts 1 and 2, respectively. Hence the first equation may be rewritten as

$$I = I_L \exp\left[-(A\rho_1 + B)\, x\right] + I_c \int_{\lambda_1}^{\lambda_2} \exp\left[-\left(\frac{k_1(\lambda)\rho_1}{\rho_{10}} + \frac{k_2(\lambda)\rho_2}{\rho_{20}}\right) x\right] d\lambda$$

where

$$\text{constant } A \text{ is } \frac{k_1(\lambda^1)}{\rho_{10}}$$

$$\text{constant } B \text{ is } \frac{k_2(\lambda^1)\rho_2}{\rho_{20}}.$$

The right-hand term will hopefully be small and is most easily handled if we expand the exponential function and neglect higher order terms:

$$I = I_L \exp\left[-(A\rho_1 + B)\,x\right] + I_c \int_{\lambda_1}^{\lambda_2} \left(1 - \frac{k_1(\lambda)\rho_1 x}{\rho_{10}} - \frac{k_2(\lambda)\rho_2 x}{\rho_{20}}\right) d\lambda$$

or

$$I = I_L \exp\left[-(A\rho_1 + B)\,x\right] + I_c\,(\lambda_2 - \lambda_1)\,[1 - (C\rho_1 + D)\,x],$$

where

$$C = \frac{1}{(\lambda_2 - \lambda_1)\,\rho_{10}} \int_{\lambda_1}^{\lambda_2} k_1(\lambda) d\lambda$$

$$D = \frac{\rho_2}{(\lambda_2 - \lambda)\rho_{20}} \int_{\lambda_1}^{\lambda_2} k_2(\lambda) d\lambda.$$

If we say that $I_c = aI_L$ (i.e., the continuous energy throughout the passband of the window is a small fraction of the energy in the Lyman-alpha line) we can write:

$$I = I_L \left\{\exp\left[-(A\rho_1 + B)\,x\right] + a(1 - C\rho_1 x - Dx)\right\}.$$

If the path length is $x = x_1$, then

$$I\,(x = x_1) = I_L \left\{a - a\,C\rho_1\,x_1 - a\,Dx_1 + \exp\left[-(A\rho_1 + B)\,x_1\right]\right\}.$$

If we vary the path length to a new value $x = x_2$, then

$$I\,(x = x_2) = I_L \left\{a - a\,C\rho_1\,x_2 - a\,Dx_2 + \exp\left[-(A\rho_1 + B)\,x_2\right]\right\}.$$

The ratio of these two quantities is

$$\frac{I\,(x = x_1)}{I\,(x = x_2)} = R = \frac{a\,[1 - x_1\,(C\rho_1 + D)] + \exp\left[-x_1\,(A\rho_1 + B)\right]}{a\,[1 - x_2\,(C\rho_1 + D)] + \exp\left[-x_2\,(A\rho_1 + B)\right]}.$$

All of the constants A, B, C, and D can be determined when ρ_2 remains constant as can the value a and distances x_1 and x_2; then the ratio $R = R\,(\rho_1)$ uniquely determines the water vapor density ρ_1 through the above transcendental equation.

It is obvious that if $a \ll 1$, the $R \approx \exp\left[(x_2 - x_1)\,A\rho_1 - B\right]$ and $\ell n\ R \approx (x_2 - x_1)\,[A\rho_1 + B]$. During calibration, a linear relationship is observed to hold between $\ell n\ R$ and ρ_1; so we may assume that a is small and that our source tube emits a strong Lyman-alpha line.

Figure A2 shows a calibration curve of the device compared with a dewpoint hygrometer. Here the natural logarithm of the ratio of the intensities is definitely related in a linear way to the water vapor density. There is evidence that the emission spectrum of the source tube changes gradually with time so that the value a may change slowly with time, making it necessary to recalibrate the instrument from time to time to obtain the correct relationship between R and the water vapor density. Nevertheless, the variable path length makes the instrument independent of the source tube strength I.

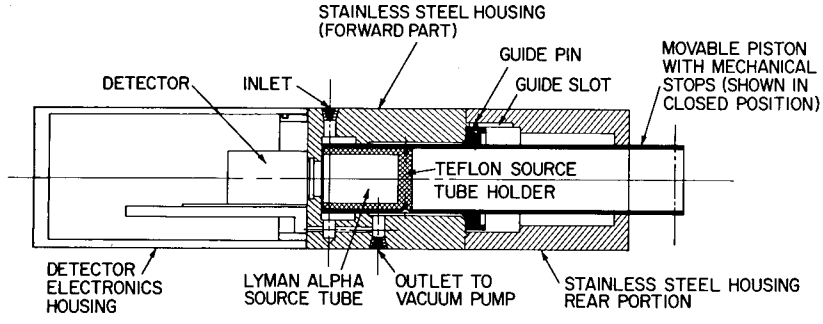

Fig. A1 — Cross-sectional view of the variable-path-length Lyman-alpha humidiometer

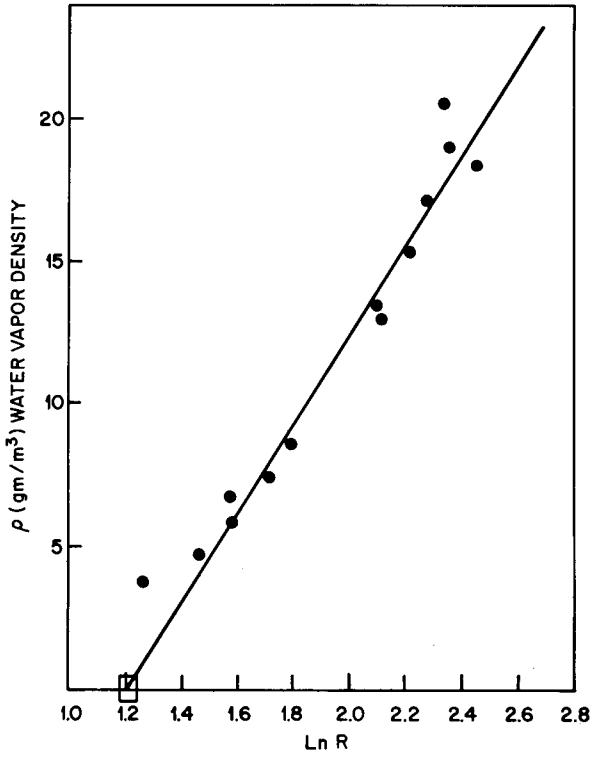

Fig. A2 — Water vapor density calibration of the Lyman-alpha humidiometer in terms of the logarithms of the ratios R of the readings for two path lengths

REFERENCES

A1. J.E. Tillman, "Water Vapor Density Measurements Utilizing the Absorption of Vacuum Ultraviolet and Infrared Radiation," in *Humidity and Moisture*, editor-in-chief, A. Wexler; Vol. 1, editor, R.E. Ruskin; Reinhold, New York, 1965, pp. 428-443.

A2. R.E. Ruskin, J.A.M. 6, 72-81 (1967).

A3. D.L. Randall, T.E. Hanley, O.K. Larison, "The NRL Lyman-Alpha Humidiometer," in *Humidity and Moisture*, editor-in-chief, A. Wexler; Vol. 1, editor, R.E. Ruskin; Reinhold, New York, 1965, pp. 444-454.